Electronic Supplementary Material (ESI) for Energy & Environmental Science.

Supplementary Information:

How simple are the models of Na-intercalation in aqueous media?

Jeongsik Yun,[1] Jonas Pfisterer,[1] Aliaksandr S. Bandarenka*,[1,2]

[1-]*Physik-Department ECS, Technische Universität München, James-Franck-Straße 1, 85748 Garching, Germany*

[2-]*Nanosystems Initiative Munich (NIM), Schellingstraße 4, 80799 Munich, Germany*

Corresponding Author: Tel. +49 (0) 89 289 12531, E-mail: bandarenka@ph.tum.de (A.S. Bandarenka)

Experimental Setup

Prior to the experiments, all glassware was cleaned with the so-called "piranha solution" (3:1 ratio of H_2SO_4 and H_2O_2) followed by subsequent rinsing with ultrapure water (18.2 MΩ, Evoqua, Germany). All experiments were performed in a typical glass cell with a three electrode setup, as shown in Figure S1. All experiments were controlled using a Bio-Logic VSP-300 potentiostat and a QCM 200 quartz crystal microbalance (Stanford Research Systems). The working electrodes, AT-cut Au quartz crystal wafers (5 MHz, 1'' diameter), were purchased from Stanford Research Systems (S_{geom} = 1.37 cm^2). The electrode potentials were referred to a Ag/AgCl (SSC) reference electrode. A Pt wire was used as a counter electrode.

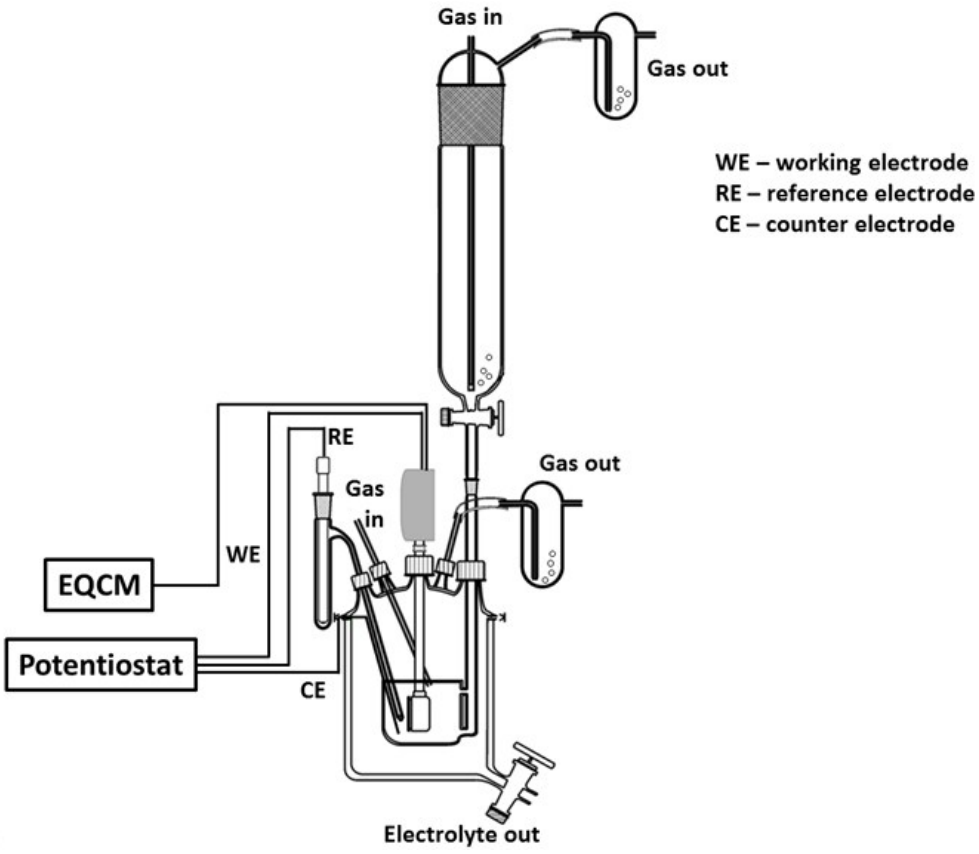

Figure S1. *Schematic representation of the 3-electrode setup used in this work [1]. The glass cell consists of inner and outer glass compartments. The inner glass chamber accommodates three electrodes, namely the working electrode (sample), the Luggin capillary of the reference electrode and the counter electrode. Before the electrolyte enters the cell, it is thoroughly deaerated in a preconditioning cell (the upper part). The outer glass compartment can be flushed by an inert gas to keep the electrolyte deaerated.*

Preparation and preconditioning

Before the deposition of the $Na_2Ni[Fe(CN)_6]$ thin films, the polycrystalline Au electrodes were electrochemically cleaned by cycling the potential between 0.2 V and 1.4 V in Ar-saturated aqueous 0.1 M $HClO_4$ solutions (d*E*/dt = 50 mV/s). The cyclic voltammograms of the polycrystalline Au electrodes in 0.1 M $HClO_4$ were characteristic to those known for polycrystalline Au electrodes (see Figure S2).

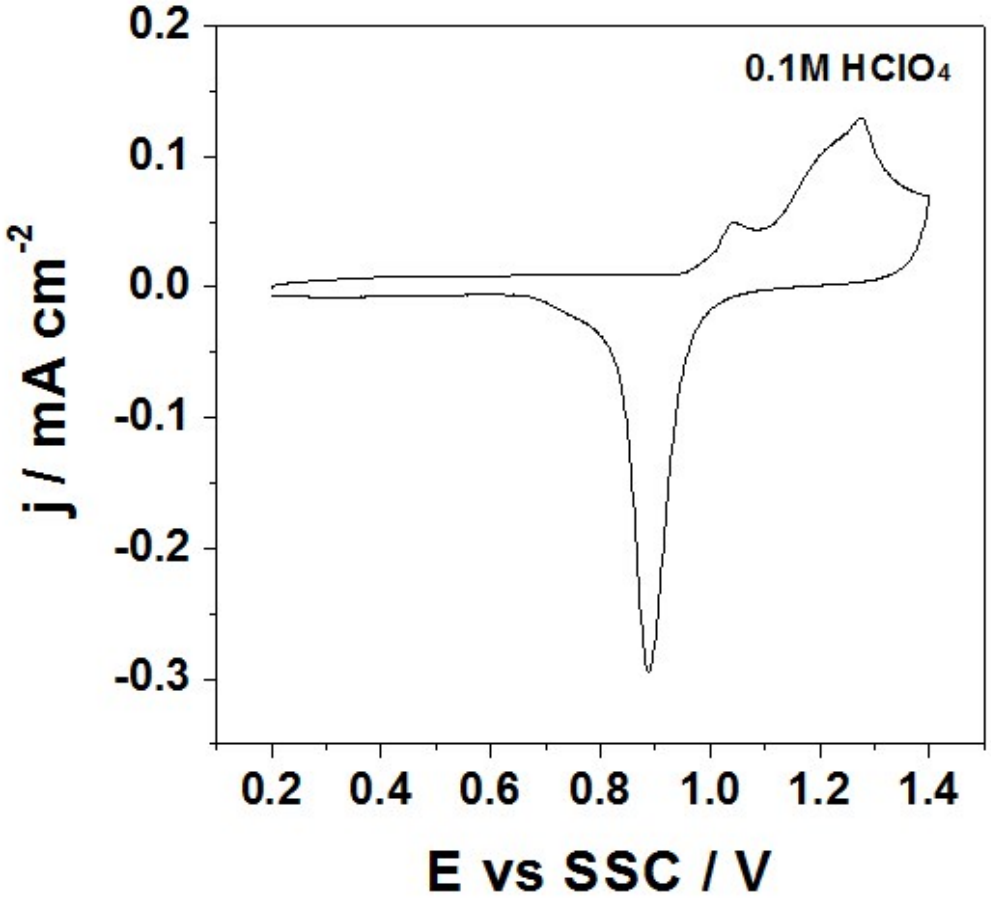

Figure S2. *A typical cyclic voltammogram of the polycrystalline Au electrode in 0.1 M $HClO_4$ during a cleaning procedure.*

Subsequently, cyclic voltammetry measurements were performed in 0.25 M Na_2SO_4 electrolytes in the potential range between 0.2 V and 1.2 V at the scan rate 50 mV/s. The cyclic voltammograms of the electrodes in aqueous 0.25 M Na_2SO_4 show, as expected, that SO_4^{2-} and OH^- ions are adsorbed on the Au electrode in the potential between 0.85 V and

1.2 V and desorbed in the potential between 0.4 V and 0.8 V, as shown in Figure S3A. The EQCM measurement shows very stable adsorption and desorption behaviour of the SO_4^{2-} and OH^- ions as shown in Figure S3B.

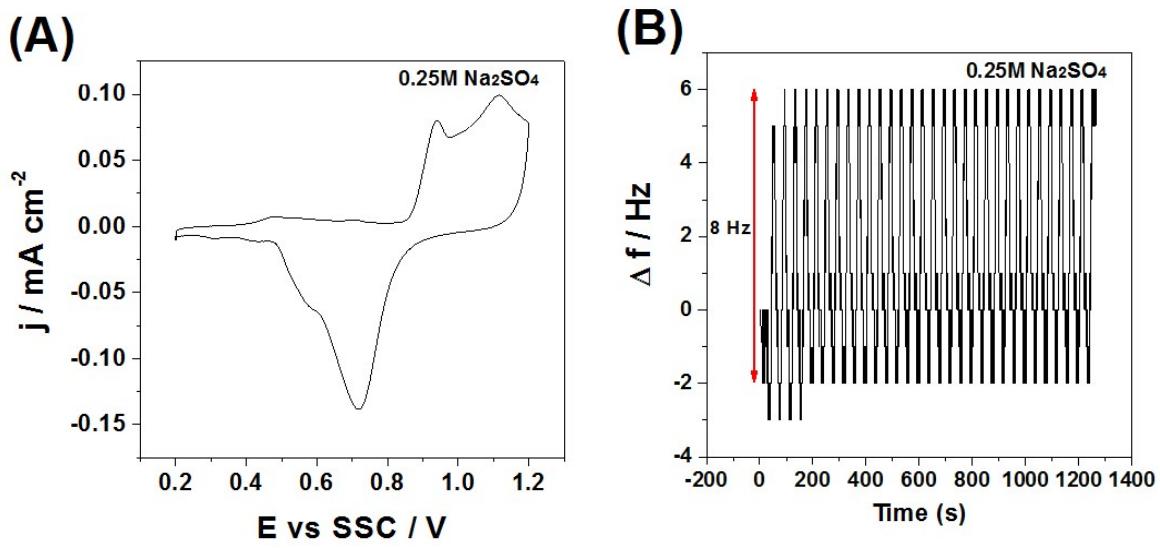

Figure S3. *(A) Typical cyclic voltammogram and (B) corresponding EQCM-curves of polycrystalline Au electrodes in 0.25 M Na_2SO_4 electrolyte before the deposition of $Na_2Ni[Fe(CN)_6]$ thin films.*

Deposition of $Na_2Ni[Fe(CN)_6]$ thin films

The $Na_2Ni[Fe(CN)_6]$ film was deposited onto the Au electrode from the solution of 0.25 M Na_2SO_4 containing 0.5 mM $K_3Ni[Fe(CN)_6]$ and 0.5 mM $NiCl_2 \cdot 6H_2O$ by cycling the potential in the range from 0.05 V to 0.85 V at the scan rate of 50 mV/s for ~60 cycles as shown in Figures 1A,B of the manuscript. Cyclic voltammetry and EQCM measurements were performed in 0.25 M Na_2SO_4 electrolytes by cycling the potential in the range between 0.05 V and 0.85 V, as shown in Figure 1C of the manuscript. Detailed characterisations of the deposited films will be given below.

Electrochemical impedance spectroscopy (EIS) measurements

EIS characterisation of $Na_2Ni[Fe(CN)_6]$ films in 0.25 M Na_2SO_4 electrolyte was conducted using AC probing frequencies between 10 kHz and 0.5 Hz with a 10 mV amplitude of the probing signals in the potential range between 0.1 V and 0.8 V. A typical admittance plot of the $Na_2Ni[Fe(CN)_6]$ thin films in 0.25 M Na_2SO_4 electrolyte is shown in Figure S4.

The output of the fitting procedure was controlled by the root-mean-square deviations and estimated individual parameter errors using home-made "EIS Data Analysis 1.0" software to ensure the validity of the model and correctness of the fitting, as described in detail elsewhere [2,3].

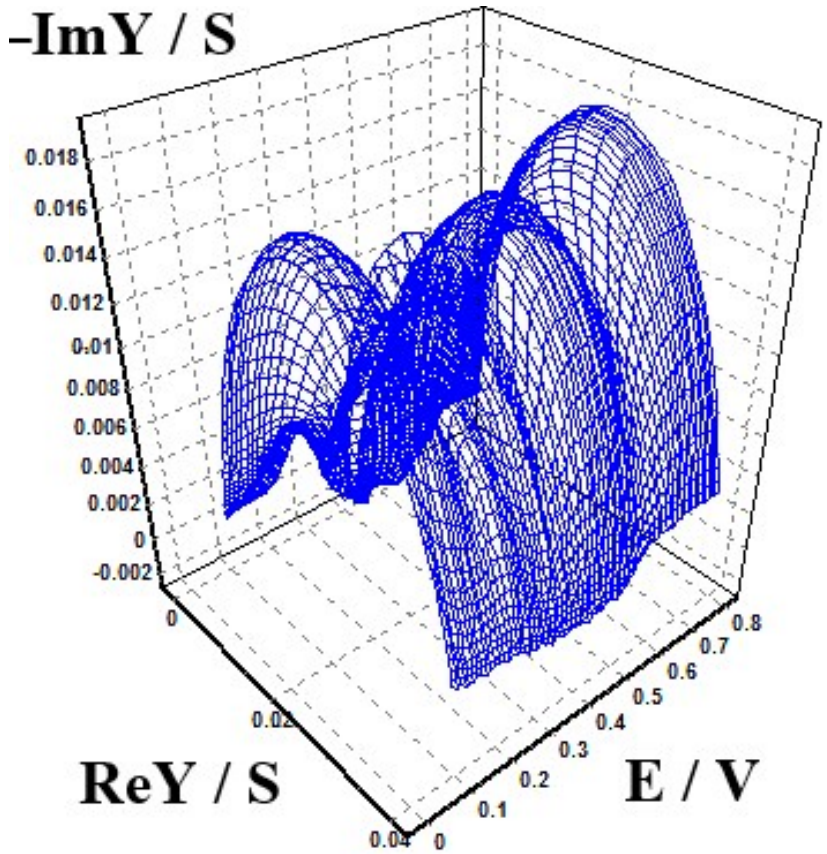

Figure S4*. A typical 3D admittance plot for the $Na_2Ni[Fe(CN)_6]$ thin films in 0.25 M Na_2SO_4.*

In the following, some further clarifications are given regarding the elucidation and use of the equivalent circuit shown in Figure 2B in the manuscript and further reproduced in

Figure S5A. Without further detailed mathematical description, which can be found in [4], the mechanism can be visualised as follows (importantly, the selected part of the equivalent circuit is just a graphical representation of parameters physically describing the adsorption processes; formally resistances and capacitances in the selected part, which are in this case just formal parameters, can be either positive or negative [4]):

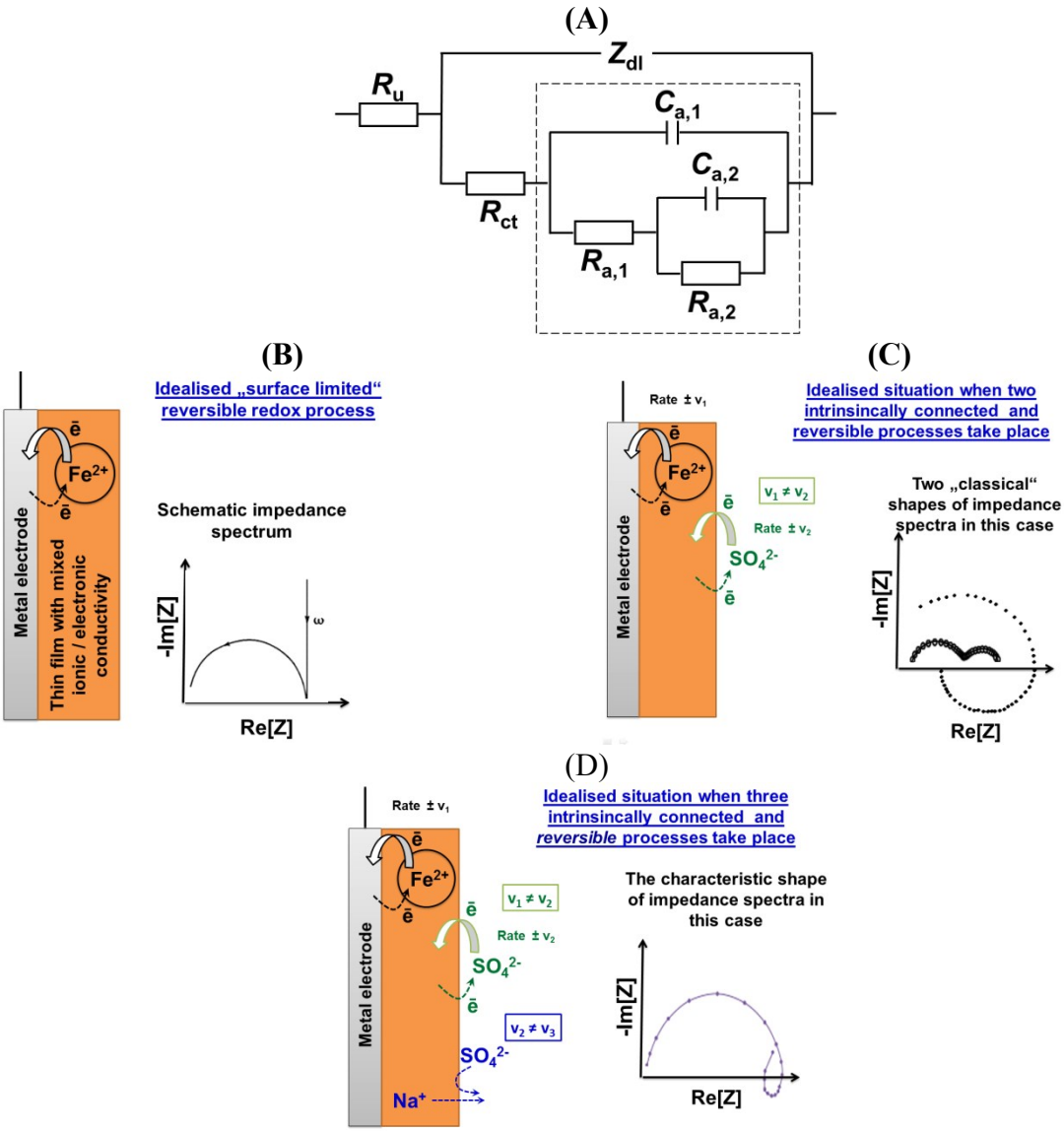

Figure S5. *(A) Equivalent electric circuit reflecting the 3-stage mechanism with three interconnected reversible stages, where each of them has different rates. (C-D) Schematics graphically illustrating how to distinguish some different mechanisms of the interfacial charge/matter transfer in electrochemical impedance spectroscopy experiments. See ref [4] for a detailed description.*

Effects of anions and cations

The difference in the "half-charged potential" ($\Delta E_{1/2}$) is defined as the potential difference between the half-charged and half-discharged states as schematically shown in Figure S6. The physical rationale to select this criterion to assess the reversibility is that, without going to the details, which can be found in the dedicated literature, adsorption and absorption processes often demonstrate energetic key points which can be further referred to this point. See for instance [5,6].

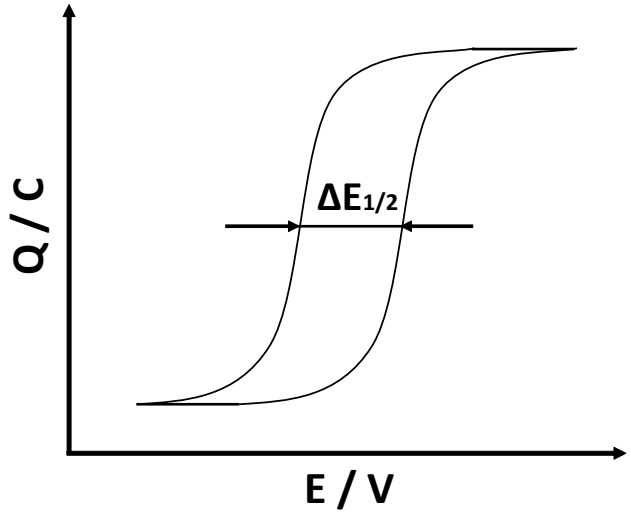

Figure S6. *Schematic description of the differences in the half-charged potentials ($\Delta E_{1/2}$), how they are defined in the manuscript text.*

Five different cyclic voltammograms and charge and discharge curves of intercalation / de-intercalation using different electrolytes were obtained as shown in Figure S7 (A) 0.25 M Na_2SO_4 (B) 0.25 M NaCl (C) 0.25 M $NaNO_3$ (D) 0.25 M $NaClO_4$ (E) 0.25 M NaOAc. The potential shifts ($\Delta E_{1/2}$) in the charging and discharging curves are significantly different. The shifts are ~59 mV, ~68 mV, ~77 mV, ~82 mV and ~102 mV for 0.25 M Na_2SO_4, 0.25 M NaCl, 0.25 M $NaNO_3$, 0.25 M $NaClO_4$ and 0.25 M NaOAc. In addition, the significant difference of the potential shifts ($\Delta E_{1/2}$) between 0.25 M Na_2SO_4 and 1 M Na_2SO_4 were found to be ~59 mV and ~15 mV respectively (see Figure 3C in the manuscript).

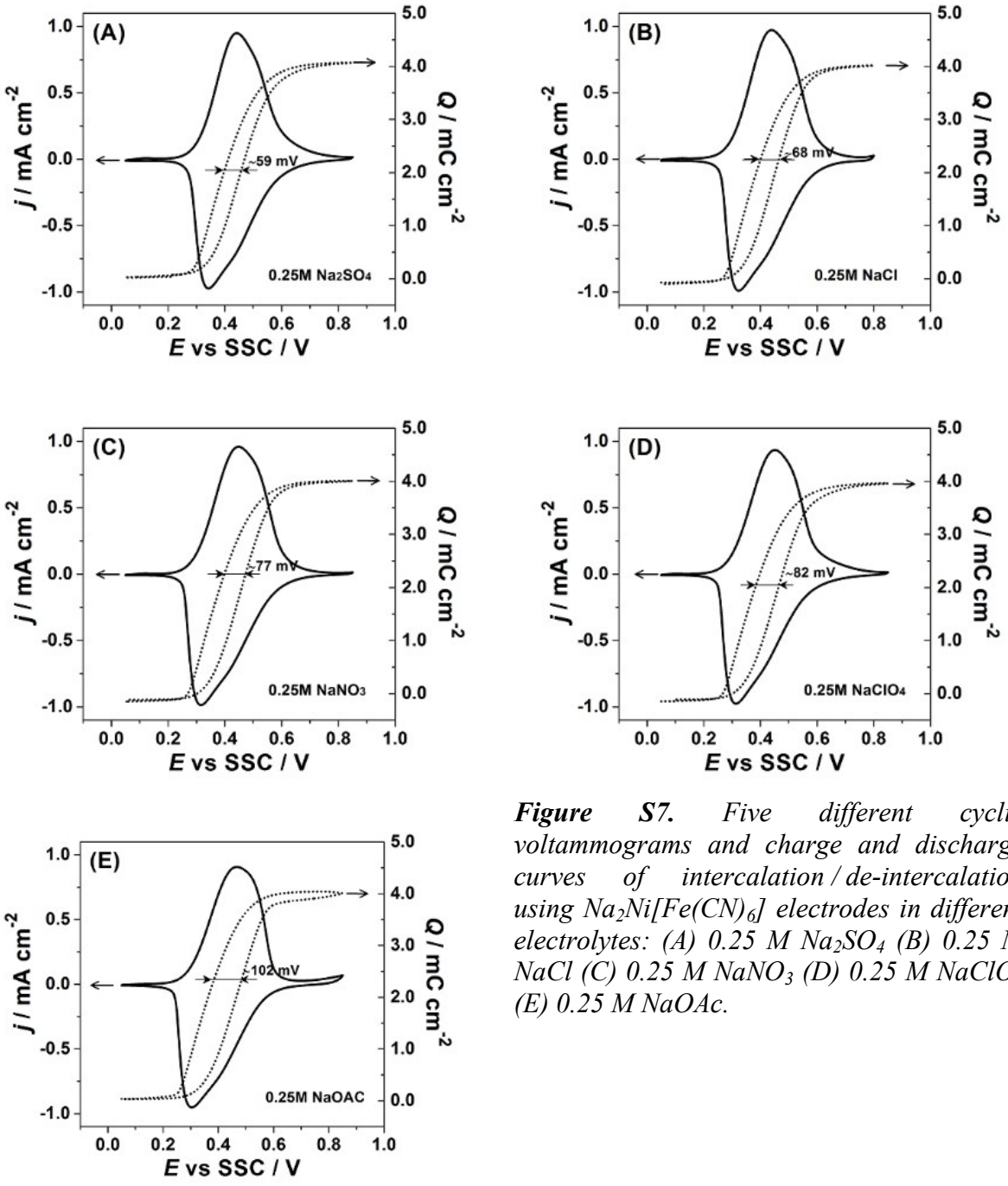

Figure S7. *Five different cyclic voltammograms and charge and discharge curves of intercalation / de-intercalation using $Na_2Ni[Fe(CN)_6]$ electrodes in different electrolytes: (A) 0.25 M Na_2SO_4 (B) 0.25 M NaCl (C) 0.25 M $NaNO_3$ (D) 0.25 M $NaClO_4$ (E) 0.25 M NaOAc.*

Battery Capacity Determination

A series of battery capacity determination (BCD) measurements was performed in order to further investigate the influence of electrolyte composition and the resulting performance of $Na_2Ni[Fe(CN)_6]$ film as one of the promising candidates of Na-ion cathode materials. At the C-rate of 180 C, the plots of cathode potential (vs a Ag/AgCl reference electrode) as a function of the specific capacity of the film utilizing different electrolytes are shown in Figure S8. Again, the potential shifts in the charging and discharging curves are significantly different. This is a measure of the system's irreversibility, which in turn corresponds to the energy efficiencies, thus portraying different performance for the different anions in the electrolyte. The "irreversibility" in Figure S8 for the 0.25 M Na_2SO_4, 0.25 M NaCl, 0.25 M $NaNO_3$, 0.25 M $NaClO_4$, 0.25 M NaOAc, electrolytes follows the same trend as in Figure 3 (in the manuscript). The specific capacity was determined to be ~80 $mAhg^{-1}$, which is, to the best of our knowledge, the highest ever reported value for this particular cathode material (assuming that the general scheme described by equation 1 takes place) [7,8].

Figure S9 shows typical galvanostatic charge and discharge curves for the $Na_2Ni[Fe(CN)_6]$ electrodes in 1 M Na_2SO_4 at different C-rates. The charging and discharging curves overlap almost completely for the C-rates of 30 C and 60 C revealing good energy efficiency. Figure S10 compares the charging and discharging curves for the $Na_2Ni[Fe(CN)_6]$ electrodes in 1 M Na_2SO_4 and 0.25 M Na_2SO_4. The higher concentration of electrolyte significantly improves the overall performance of the studied system.

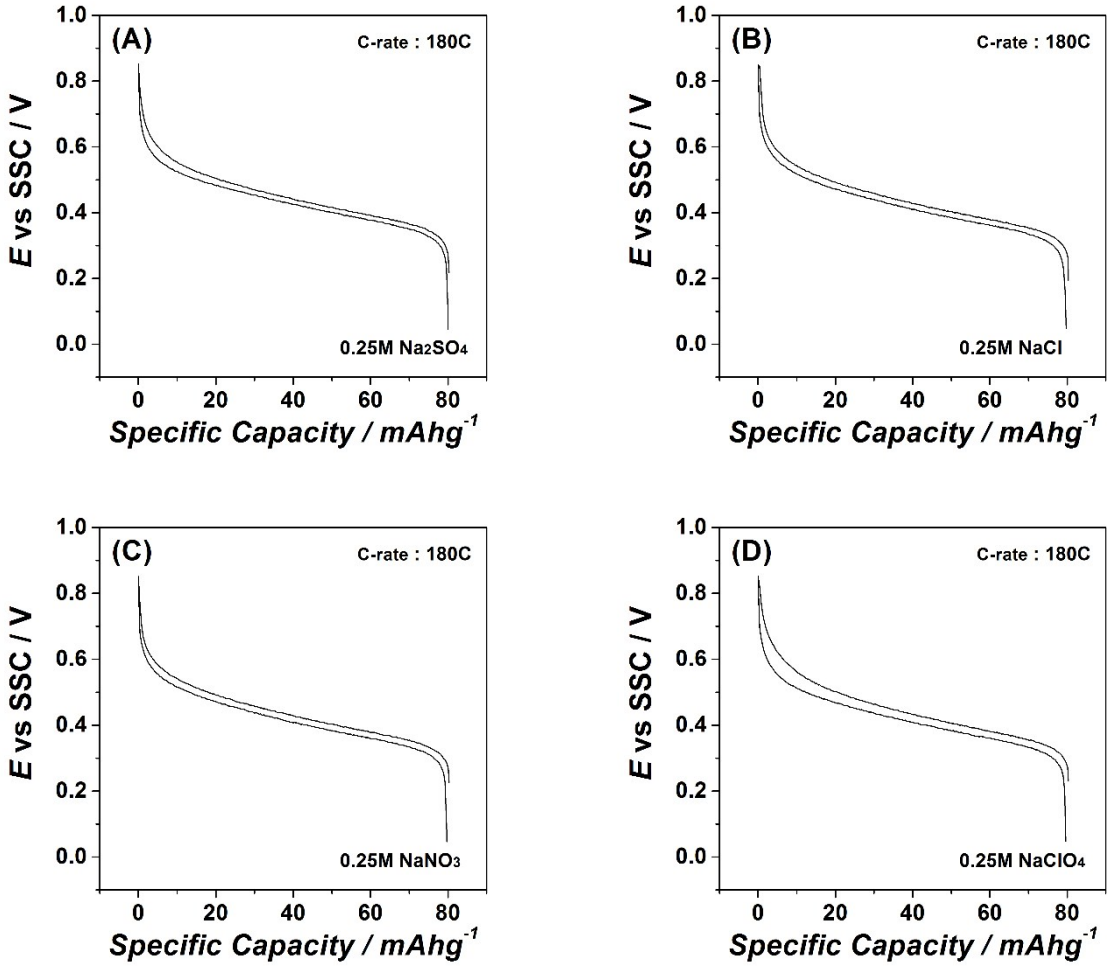

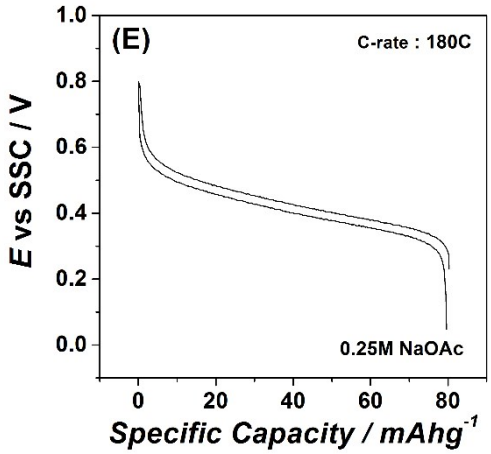

Figure S8. *Galvanostatic charge and discharge curves at 180 C for $Na_2Ni[Fe(CN)_6]$ electrodes in different electrolyte compositions, namely: (A) 0.25 M Na_2SO_4 (B) 0.25 M NaCl (C) 0.25 M $NaNO_3$ (D) 0.25 M $NaClO_4$ (E) 0.25 M NaOAc.*

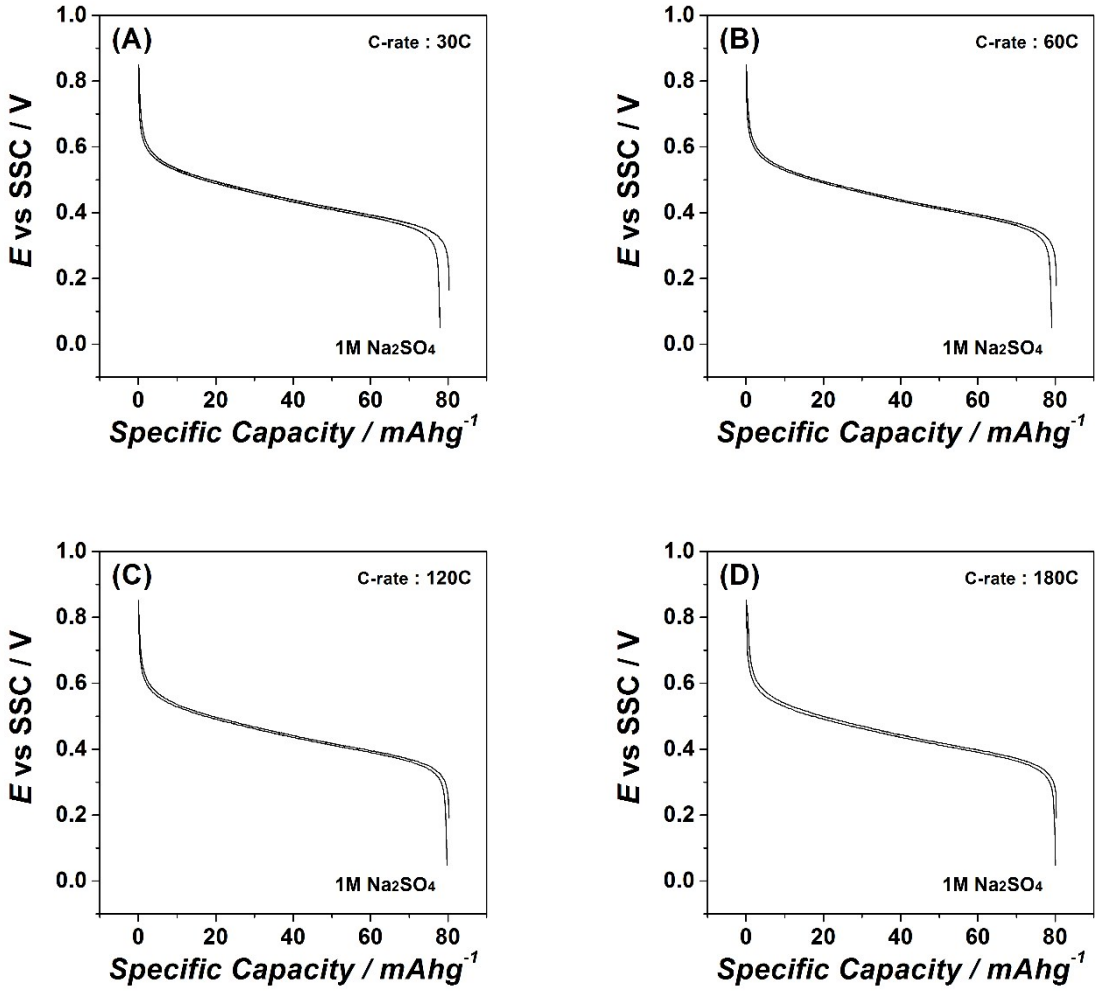

Figure S9. *Galvanostatic charge and discharge curves for $Na_2Ni[Fe(CN)_6]$ electrodes in 1 M Na_2SO_4 at different C-rates: (A) 30 C, (B) 60 C, (C) 120 C and (D) 180 C.*

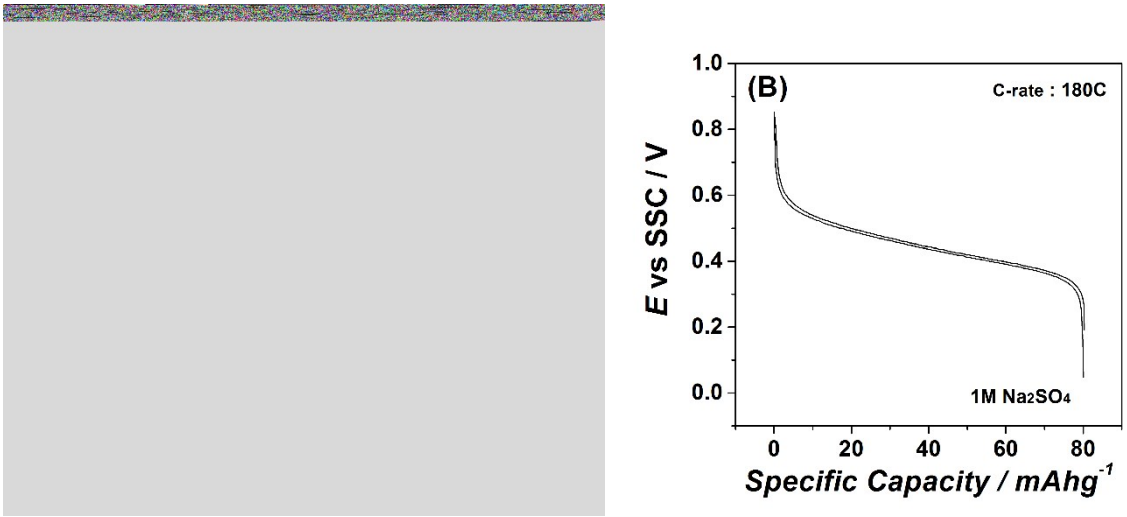

Figure S10. *Galvanostatic charge and discharge curves for $Na_2Ni[Fe(CN)_6]$ electrodes in (A) 0.25 M Na_2SO_4 and (B) 1 M Na_2SO_4 aqueous electrolytes.*

AFM Measurements

The Atomic Force Microscope (AFM), utilized in this work, was a multimode EC-STM/AFM instrument (Veeco VI) with a Nanoscope IIID controller using the Nanoscope 5.31r1 software. All measurements were conducted in tapping mode (AFM-tips purchased from BRUKER RTESP-300). The AFM was placed on an air table (Newport) to reduce vibrations. The recorded images were analysed by the WSxM 5.0 Develop 8.0 software [9].

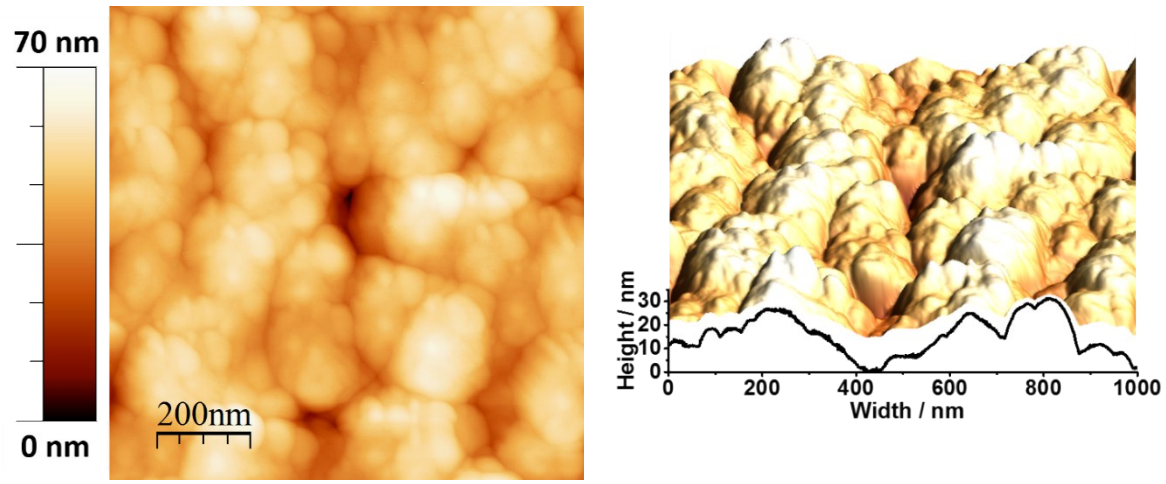

Figure S11. *AFM image (left) and its three dimensional illustration (right) of electrochemically deposited* $Na_2Ni[Fe(CN)_6]$ *film on polycrystalline Au. The surface structure appears to be rather uniform.*

Firstly, the $Na_2Ni[Fe(CN)_6]$ thin film, electrochemically deposited on polycrystalline Au electrode (as discussed above), was imaged by AFM. For this purpose, the sample was carefully fractured in order to obtain a suitable sample size compatible for AFM measurements. Thereafter, the sample was tightly attached with a double sided adhesive tape to a magnetic metal plate (used as a sample holder), which was then put on the sample stage of the AFM. Different regions of the surface were investigated by utilizing different scan sizes (5x5μm, 1x1μm, 500x500nm). A typical recorded picture, together with a three dimensional representation, is shown in Figure S11. The surface structure seems to be rather uniform; however, it is quite difficult to differentiate from polycrystalline Au. Therefore, additional experiments were conducted using a single crystal substrate to further elucidate the surface morphology.

As a substrate, a Pt(110) single crystal (MaTecK, Ø=5mm) was cleaned in a "piranha solution" (3:1 mixture of H_2SO_4 and H_2O_2) for 20 min and then prepared according to the standard procedure developed by Clavilier et al. [10]. The Pt(110) was annealed to approximately 1000°C and subsequently cooled in Ar/CO-atmosphere (CO 1000ppm, Ar rest, purity 4.7/5.0, Westfalen AG) in order to achieve a flat and well-ordered substrate [11].

Before the $Na_2Ni[Fe(CN)_6]$ film was electrochemically deposited onto the Pt(110) substrate, reference images were attained by AFM (see Figure 1D and Figure S12). The Pt(110) was again tightly attached to the magnetic sample holder and different regions of the single crystal were examined for uniformity and flatness exploiting different scan sizes (5x5µm, 500x500nm).

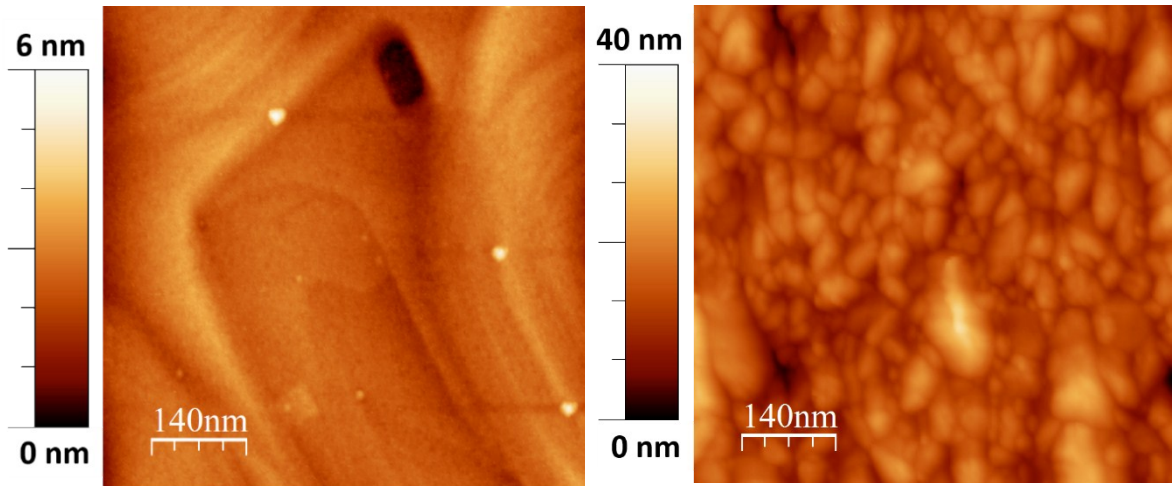

Figure S12. *Comparison of AFM images taken before (left) and after (right) the film deposition on the single crystal Pt(110). Compare to Figures 1D,E for 3D representations and line profiles. The bare Pt(110) exhibits step edges and is flat, thus representing an ideal substrate for thin film characterization. The surface of the deposited thin film seems fairly uniform with a height profile of only 40nm.*

The electrochemical deposition of the $Na_2Ni[Fe(CN)_6]$ films onto the Pt(110) single crystal was performed in a typical electrochemical glass cell exploiting a three electrode setup as described above. The electrolyte was composed of 0.25 M Na_2SO_4, 0.5 mM $K_3Fe(CN)_6$ and 0.5 mM $NiCl_2 \cdot 6H_2O$ (Purity of all chemicals are stated below). The electrolyte was purged by Ar gas (purity 5.0) for 15 min prior to the experiments. For film deposition ~60 cycles were performed in a potential range from 50 mV to 700 mV vs. a Ag/AgCl reference electrode at the scan rate of 50 mV/s. After the deposition, the film was thoroughly rinsed with ultrapure water and dried. Subsequently, the sample was again mounted on the magnetic

sample holder and investigated by AFM (see Figures 1E,F and Figure S12). Different scan sizes and positions were imaged to ensure overall sample uniformity.

SEM and Electron Microprobe Measurements

SEM and Electron Microprobe images were obtained with a 20 kV beam using "Mira" from Tescan, Czech Republic with electron microprobe "INCA Energy 350" from Oxford Instruments Analytical, UK. As shown in Figure S13-15 Na, Ni and Fe are uniformly distributed, which indicates that the $Na_2Ni[Fe(CN)_6]$ film was uniformly deposited.

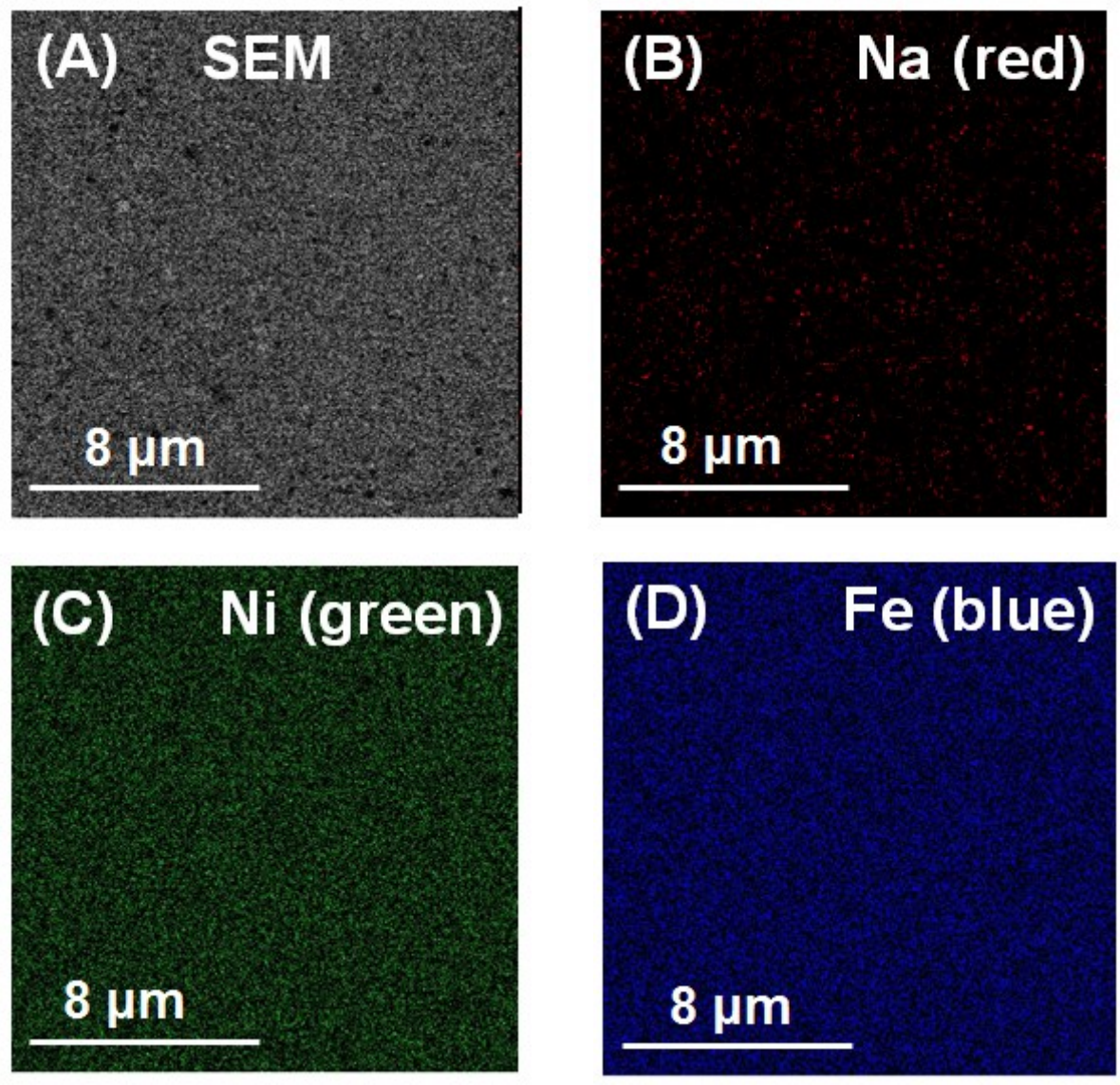

Figure S13. *SEM and Electron Microprobe images of the $Na_2Ni[Fe(CN)_6]$ film.*

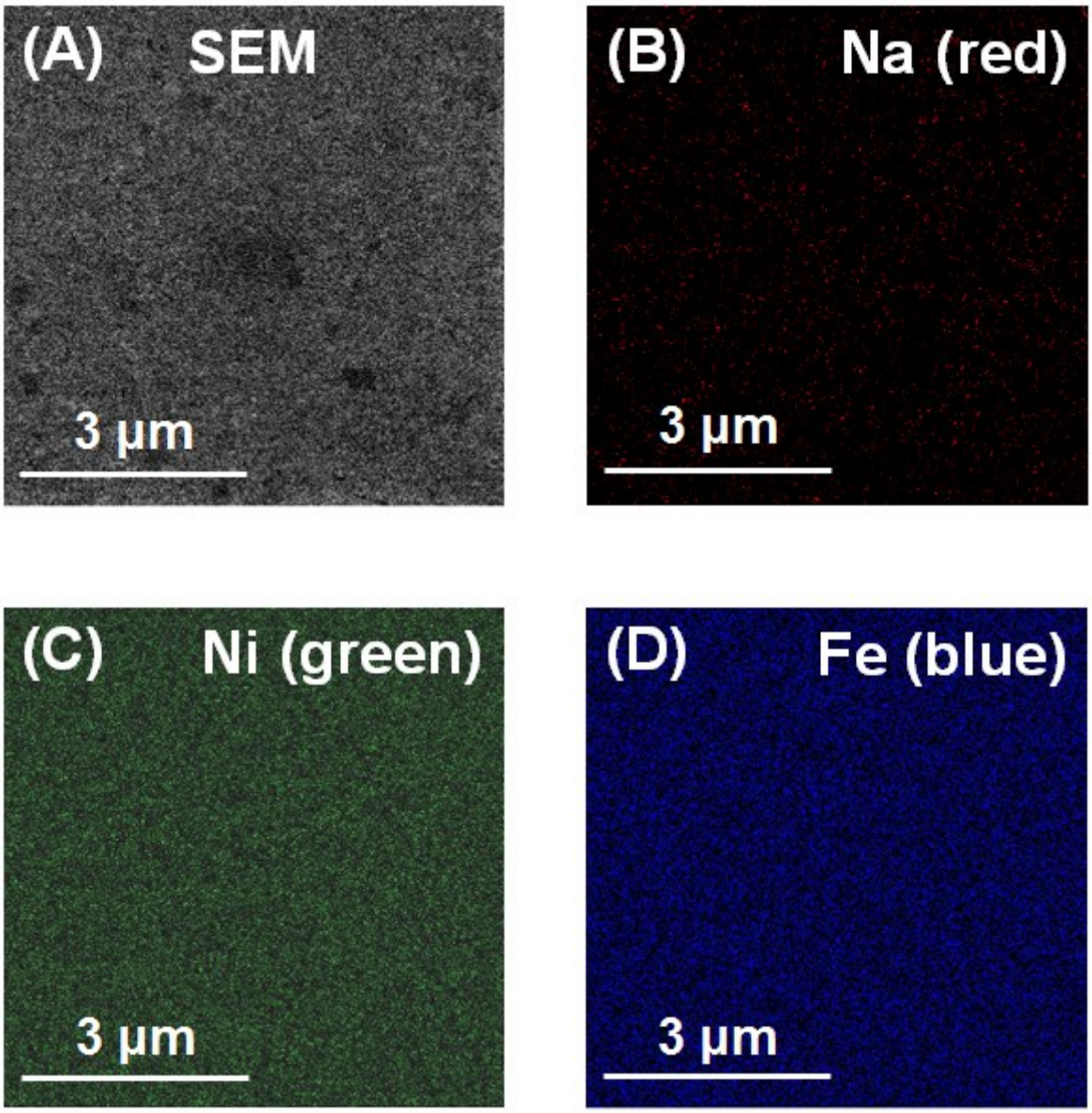

Figure S14. *SEM and Electron Microprobe images of the $Na_2Ni[Fe(CN)_6]$ film.*

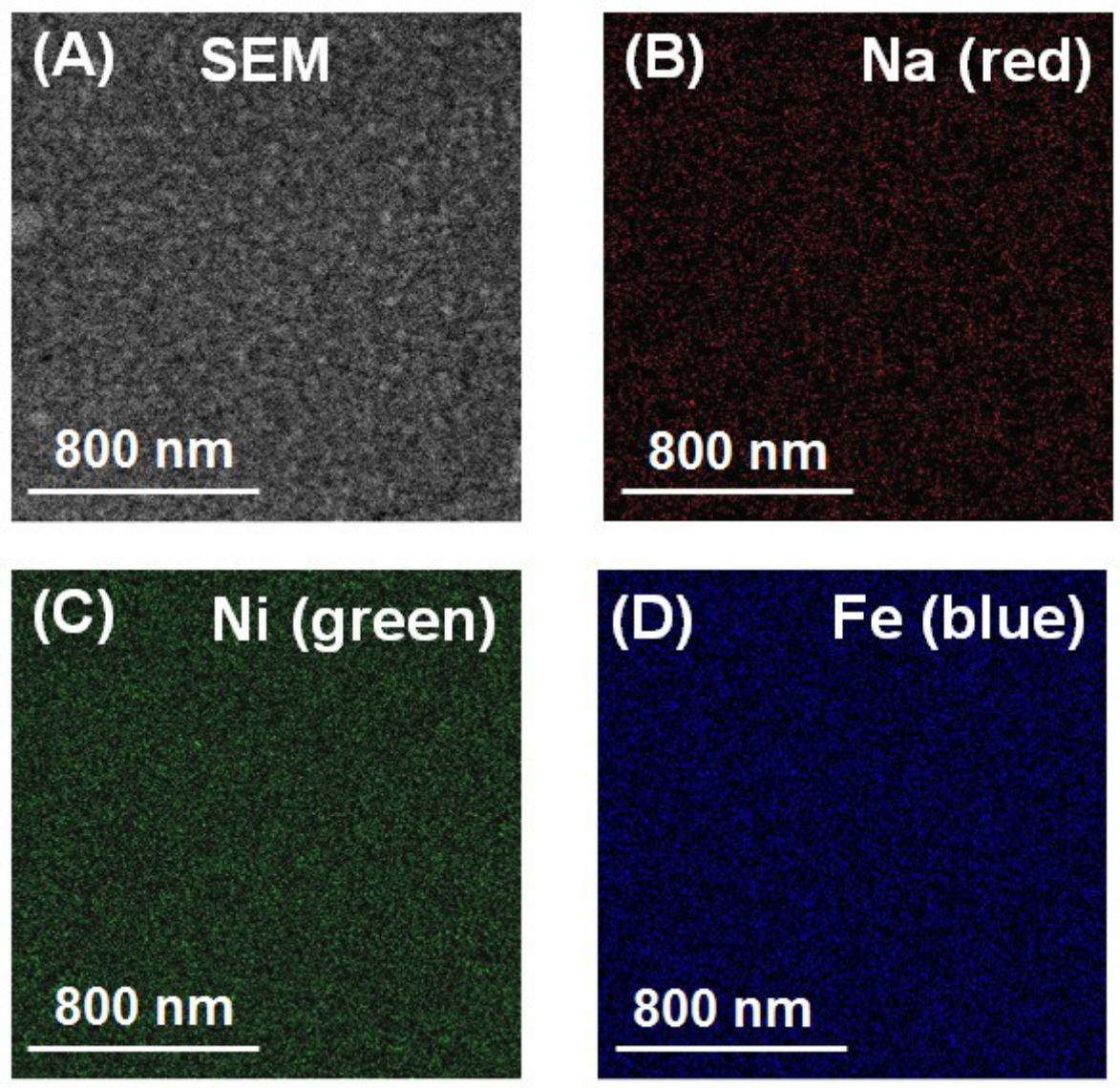

Figure S15. *SEM and Electron Microprobe images of the $Na_2Ni[Fe(CN)_6]$ film.*

Chemicals

$K_3Ni[Fe(CN)_6]$ (99%, Sigma Aldrich, Germany), $NiCl_2 \cdot 6H_2O$ (99.3%, Alfa Aesar, Germany) Na_2SO_4 (99.0%, Sigma Aldrich, Germany), NaCl (99.0%, Sigma Aldrich, Germany), NaOAc (99%, Sigma Aldrich, Germany), $NaClO_4 \cdot H_2O$ (98%, Sigma Aldrich, Germany), K_2SO_4 (99.0%, Sigma Aldrich, Germany), KCl (99%, Sigma Aldrich, Germany), $LiNO_3$ (ReagentPlus®, Sigma Aldrich, Germany), $NaNO_3$ (99.0%, Sigma Aldrich, Germany), KNO_3 (99.0%, Sigma Aldrich, Germany), $RbNO_3$ (99.7%, Sigma Aldrich, Germany), $CsNO_3$ (99%, Sigma Aldrich, Germany)

References

1. Berkes et al., *J. Phys. Chem. C* 2011, **115**, 9122.

2. A.S. Bondarenko, *Anal. Chim. Acta*, 2012, **743**, 41.

3. A.S. Bondarenko and G. A. Ragoisha, in Progress in Chemometrics Research, ed. A. L. Pomerantsev, 2005, pp. 89–102.

4 A. Lasia, Electrochemical Impedance Spectroscopy and its Applications, Springer-Verlag New York, 2014, 367.

5. J. Rossmeisl, G. S. Karlberg, T. Jaramillo and J. K. Nørskov, *Faraday Discussions*, 2008, **140**, 337.

6. A.S. Bondarenko, H.A. Hansen, J. Rossmeisl, I. Stephens, *Phys. Chem. Chem. Phys*. 2014, **16**, 13625.

7. Y. F. Yue, A. J. Binder, B. K. Guo, Z. Y. Zhang, Z. A. Qiao, C. C. Tian and S. Dai, *Angewandte Chem. Int. Ed*., 2014, **53**, 3134.

8. Y. You, X. L. Wu, Y. X. Yin and Y. G. Guo, *J. Mater. Chem. A*, 2013, **1**, 14061.

9. I. Horcas, R. Fernández, J. M. Gómez-Rodríguez, J. Colchero, J. Gómez-Herrero, and A. M. Baro, *Rev. Sci. Inst*., 2007, **78**, 013705.

10. J. Clavilier, R. Faure, G. Guinet and R. Durand, *J. Electroanal. Chem*., 1980, **107**, 205.

11. L. A. Kibler, A. Cuesta, M. Kleinert, D. M. Kolb, *J. Electroanal. Chem*., 2000, **484**, 73.